

Effective Pressure Law for Permeability of Westerly Granite Under Cyclic Loading

C. A. MORROW

U.S. Geological Survey, Menlo Park, California

ZHANG BO-CHONG

State Seismological Bureau, Beijing, Peoples' Republic of China

J. D. BYERLEE

U.S. Geological Survey, Menlo Park, California

The permeability of Westerly granite was measured under cyclic loading conditions for confining pressures P_c to 96 MPa and pore pressures P_p to 86 MPa in order to determine the coefficient α of the effective pressure equation $P_e = P_c - \alpha P_p$, where P_e , P_c , and P_p are effective, confining, and pore pressures, respectively. Two methods of determining α are described, based on the cubic root law, $k^{1/3} = A + B \ln(P_e)$, which relates permeability k to effective pressure in fractures. A and B of this equation are functions of the geometric parameters of the cracks; α was close to 1 under all conditions of pressure and loading history. Pressure cycling had significant effects on the permeability of the granite, as demonstrated by the large variations in the coefficients A and B of the cubic root law.

INTRODUCTION

The permeability of porous and jointed rock is greatly affected by both internal fluid pressure and external loading, whether from overburden or tectonic forces. In order to understand the complex process of fluid flow through geologic materials under stress, we need to begin with the basic models for flow through simple fractures. In a comprehensive work on laminar flow through glass plates (representing fracture surfaces), *Lomize* [1951] showed that the flow rate was proportional to the cube of the aperture dimension. That is,

$$Q = \frac{(2a)^3}{12\mu} \left(\frac{dP}{dl} \right) \quad (1)$$

where Q is flow rate, a is aperture half width, μ is the viscosity of the pore fluid, and dP/dl is the pore pressure gradient across the length of the sample. This "cubic law" has been studied by numerous workers and modified to incorporate the effects of nonparallel plates, wall roughness, asperity contact, and fractures under normal stress. See, for instance, *Louis* [1969], *Bear* [1972], *Witherspoon et al.* [1980], *Gangi* [1978], and *Walsh* [1981].

Darcy's law relates permeability to fluid flow:

$$k = - \frac{Q\mu}{A_s} \left(\frac{dl}{dP} \right) \quad (2)$$

where k is permeability, A_s is the cross-sectional area of the sample, and other variables are defined as above. Since $(2a)^3$ is proportional to Q from (1) and k is proportional to Q from (2), then it follows that "a," the aperture half width, is proportional to $k^{1/3}$. *Jones* [1975] and *Brar and Stesky* [1980] demonstrate this relation on artificial fractures of various rock types. Crack half width a is also dependent on confining pressure P_c , and so they show empirically that $k^{1/3}$ is proportional to log

P_c . *Walsh* [1981] derived this relation analytically, based on the theory of compressible fractures given by *Walsh and Grosenbaugh* [1979]. His derivation includes the effect of variable pore pressure and is written as

$$(k/k_0)^{1/3} = 1 - (2^{1/2}h/a_0) \ln(P/P_0)_e \quad (3)$$

or

$$k^{1/3} = k_0^{1/3} - k_0^{1/3}(2^{1/2}h/a_0) \ln(P/P_0)_e \quad (4)$$

where k is permeability, k_0 is the permeability at a reference pressure P_0 , h is the root-mean-square height distribution of the asperities in a fracture, a_0 is the aperture half width at some reference pressure P_0 , and P is pressure. The subscript e refers to effective pressure P_e , which is defined as

$$P_e = P_c - \alpha P_p \quad (5)$$

Effective pressure for permeability is often considered merely the difference between confining pressure and pore pressure $P_c - P_p$. However, some studies have shown that α may take on values other than 1. For instance, α was found to be 0.56 or 0.91 for jointed Barre Granite with different surface roughness conditions [*Walsh*, 1981], 0.6-0.7 for intact Chelmsford Granite [*Bernebe et al.*, 1984], and 2.2 or 4.0 for Berea Sandstone, depending on bedding orientation [*Zoback and Byerlee*, 1975].

In this work we begin with equation (4) rewritten in the general form

$$k^{1/3} = A + B \ln(P_c - \alpha P_p) \quad (6)$$

where A and B are functions of the geometric parameters of the cracks, in order to address a number of questions concerning the permeability of granitic rocks. First, is the "cubic root" equation, as we shall call (6), appropriate for describing flow through intact samples? What are the best methods for determining the coefficient α , and finally, what are the effects of stress cycling on the permeability of granite? To answer these questions, we have performed a series of permeability experiments on intact samples of Westerly granite.

Copyright 1986 by the American Geophysical Union.

Paper number 4B5384.
0148-0227/86/004B-5384\$05.00

TABLE 1. Permeability Values ($\pm 2\%$)

P_c , MPa	P_p , MPa	k , ($m^2 \times 10^{-21}$)	$k^{1/3}$, $m^2 \times 10^{-7}$
<i>Sample 3</i>			
96	6	7.39	1.95
96	26	12.13	2.30
96	46	14.77	2.45
96	66	25.32	2.94
96	86	70.69	4.14
11	1	50.00	3.68
16	6	44.84	3.55
36	6	14.77	2.45
36	26	40.62	3.44
56	6	6.86	1.90
56	26	13.19	2.36
56	46	30.60	3.13
76	6	0.65	0.87
76	26	2.11	1.28
76	46	4.01	1.59
76	66	13.29	2.37
<i>Sample 4</i>			
96	1	21.10	2.76
96	26	33.76	3.23
96	46	41.67	3.47
96	66	58.55	3.88
96	86	135.04	5.13
96	66	61.19	3.94
96	46	37.45	3.35
96	26	26.38	2.98
96	1	18.99	2.67
96	26	27.43	3.02
96	46	33.76	3.23
96	66	51.70	3.73
96	86	111.83	4.82
96	66	53.28	3.76
96	46	34.29	3.25
96	26	24.27	2.90
96	1	15.83	2.51
96	26	22.68	2.83
96	46	29.54	3.09
96	66	44.31	3.54
96	86	105.50	4.73
96	66	44.31	3.54
96	46	29.01	3.07
96	26	19.52	2.69
96	1	14.24	2.42
56	1	25.32	2.94
56	26	40.09	3.42
56	46	78.07	4.27
56	26	36.93	3.33
56	1	22.16	2.81
56	26	34.82	3.27
56	46	71.74	4.16
56	26	34.29	3.25
56	1	22.68	2.83
56	26	32.18	3.18
56	46	70.68	4.13
56	26	32.18	3.18
56	1	21.10	2.76
16	1	45.37	3.57
16	6	56.44	3.84
16	1	46.95	3.61
16	6	57.50	3.86
16	1	49.06	3.66
16	6	56.44	3.84
16	1	47.48	3.62
56	1	6.33	1.85
56	26	12.66	2.33
56	46	34.82	3.27
56	26	11.61	2.26
<i>Sample 4 (Retested After 2 Weeks)</i>			
96	1	17.41	2.59
96	46	30.07	3.11
96	66	42.20	3.48
96	86	107.61	4.76
56	1	23.21	2.85

TABLE 1. (continued)

P_c , MPa	P_p , MPa	k , ($m^2 \times 10^{-21}$)	$k^{1/3}$, $m^2 \times 10^{-7}$
<i>Sample 4 (Retested After 2 Weeks) (continued)</i>			
56	26	40.09	3.42
56	46	84.40	4.39
16	1	59.61	3.91
16	6	72.80	4.18
56	1	23.74	2.87
56	26	38.51	3.38
56	46	81.24	4.33
96	1	12.66	2.33
96	46	25.32	2.94
96	66	40.09	3.42
96	86	98.12	4.61
<i>Sample 6</i>			
16	1	30.33	3.12
56	1	6.86	1.90
96	1	3.43	1.51
56	1	6.07	1.82
16	1	19.78	2.70
56	1	5.01	1.71
96	1	1.85	1.23
56	1	4.62	1.67
16	1	5.49	2.49

PROCEDURE

Cylindrical samples of Westerly granite were prepared, 2.54 cm in diameter and 2.54 cm long. These samples were placed between two highly permeable spacers to allow uniform flow of water at the rock interfaces. This assembly was then jacketed in polyurethane tubing and attached to steel end plugs, as shown in Figure 1. Confining pressure was maintained by a computer-controlled servomechanism. Pore pressure was held constant by a fluid accumulator at the outlet side of the system. Inlet and outlet fluid pressures were monitored by two identical pressure transducers. The difference between the two signals (the pressure drop across the sample) was used to activate a small intensifier, which maintained the inlet pressure at 2 MPa above the back pressure. Steady state flow was established through the sample for periods of up to 8 hours to ensure flow equilibrium. A controlled temperature

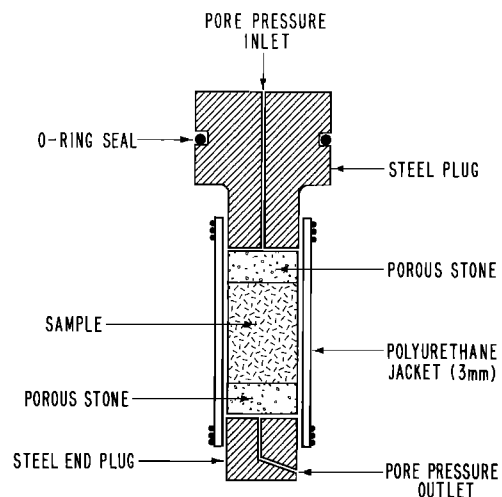


Fig. 1. Sample assembly. A cylindrical sample is capped at either end with highly permeable porous stones, which allow fluids to flow uniformly into or out of the rock. Steady state flow of water is established due to a fixed pore pressure gradient across the sample.

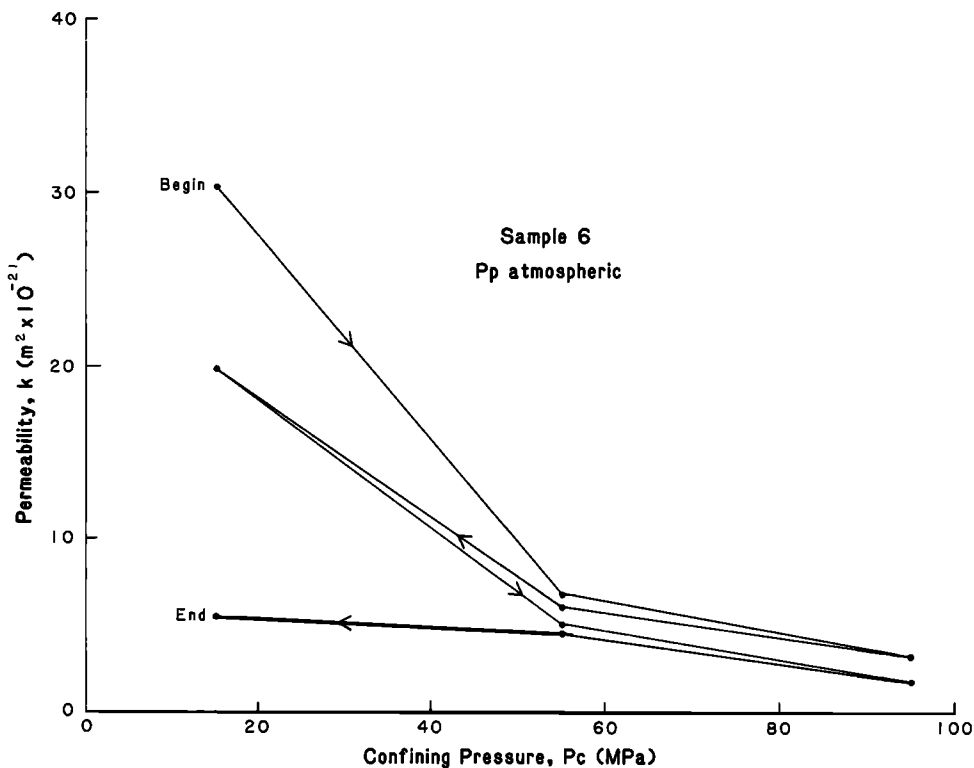


Fig. 2. Permeability as a function of confining pressure for sample 6 during two cycles of loading and unloading. Pore pressure remained atmospheric during each measurement. Arrows indicate the order of the experiments, beginning with the upper left-most data point.

($27 \pm 0.5^\circ\text{C}$) was required for accurate fluid flow measurements. Deionized water served as the pore fluid in all tests.

Permeability k was determined by measuring the volume of fluid which passed through the sample with time due to a fixed pore pressure gradient. Using Darcy's law (equation (2)) with $A_s = 5.07 \text{ cm}^2$, $\mu = 0.8445 \text{ dyn s/cm}^2$, $dP = 20.26 \text{ atm}$, and $dl = 2.54 \text{ cm}$, we get

$$k = 0.0211Q$$

with flow rate Q , in cubic centimeters per second and k in darcies ($1 \text{ darcy} = 0.987 \times 10^{-12} \text{ m}^2$).

Experiments were designed to test the effects of confining pressure cycling (samples 3 and 6) and pore pressure cycling (sample 4) on the permeability of the granite. For this reason, each sample was run through a different loading history (see Table 1). All data are listed in consecutive experimental order. All permeability values are $\pm 2\%$.

RESULTS

The permeability of sample 6 is shown in Figure 2 as a function of confining pressure. These measurements were all made with atmospheric pore pressure at the outlet of the

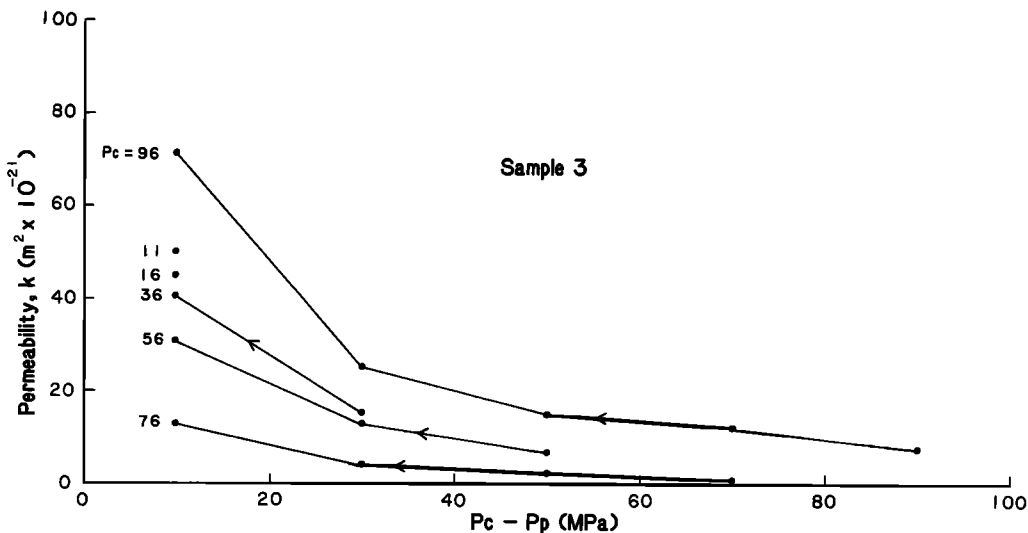


Fig. 3. Permeability as a function of pressure difference $P_c - P_p$ for sample 3. Arrows indicate the direction of loading. Confining pressures are listed at left. For $P_c = 11$ and 16 MPa , only one permeability measurement was made; these data are shown as single points.

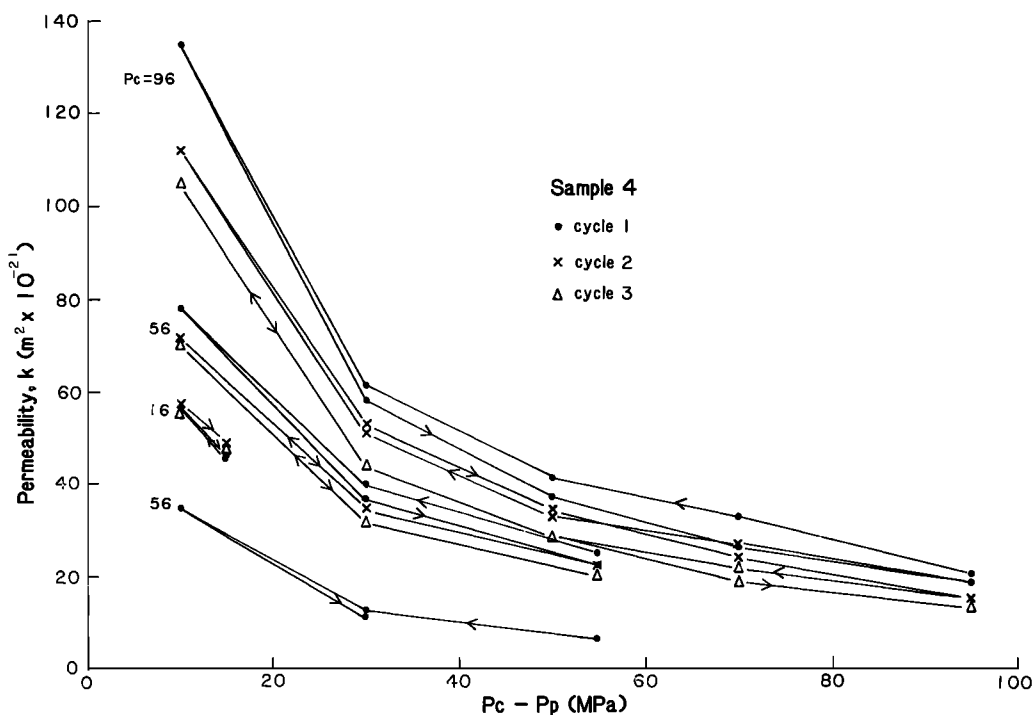


Fig. 4. Permeability as a function of pressure $P_c - P_p$ for sample 4. Confining pressures are listed at left, and loading paths are shown with arrows. At a confining pressure of 96 MPa, pore pressure was cycled three times, as indicated by the three different symbols within each confining pressure group. This process was repeated at confining pressures of 56 and 16 MPa. Confining pressure was then raised to 56 MPa for one pore pressure cycle. The order of these experiments is from top to bottom of the figure.

sample. The sequence of permeability measurements is shown with arrows, beginning at the top left of Figure 2 with an initial permeability of $30.33 \times 10^{-21} \text{ m}^2$ at a confining pressure of 16 MPa. Permeabilities ranged between 10^{-21} and 10^{-20} m^2 , decreasing slightly at the higher confining pressures because the crack apertures diminished with applied pressure. Each stress cycle resulted in lower permeability values than the one before, indicating that the cracks did not reopen to their original state immediately after the stress was released. Repeated runs of this experiment with different samples gave identical results.

The permeability of sample 3 was measured sequentially at confining pressures of 96, 11, 16, 36, 56, and 76 MPa. The pore pressure was raised in intervals of 20 MPa for each series of confining pressure measurements. Data are shown in Figure 3 as a function of pressure difference $P_c - P_p$, with the order of measurements indicated by arrows. Initial measurements begin at the right of Figure 3 (96 MPa); final values are at the bottom left (76 MPa). This plot has many of the features of Figure 2; permeability decreased at the higher pressure differences, and each successive loading cycle resulted in lower permeabilities. This reduction occurred regardless of the confining pressure; note that permeability decreased from 96 to 11 MPa, contrary to what we might expect based on elastic models of crack closure. Over the course of the experiments, permeability decreased from 70×10^{-21} to $13 \times 10^{-21} \text{ m}^2$ at a pressure difference of 10 MPa.

The loading history of sample 4 is the most complex and was designed to test the effects of pore pressure cycling. With confining pressure fixed at 96 MPa, pore pressures were varied from low to high values three times, measuring permeability after each pore pressure step. This process was repeated at confining pressures of 56 and 16 MPa, and then back to 56

MPa. Data are shown in Figure 4, with the order of experiments indicated by arrows, beginning at the right-hand side of the uppermost curve. Even when confining pressure remained constant, each successive cycle had a lower permeability curve, indicating that there was some change in the rock after every loading. Permeability also decreased as confining pressures were lowered. This trend continued even when P_c was raised from 16 to 56 MPa, creating two completely different sets of permeability values at 56 MPa for this sample.

After a hiatus of 2 weeks (in which the sample was held at atmospheric P_c and P_p), additional permeability measurements were made on sample 4 in order to test for time-dependent behavior. During these runs, pore pressure was applied only once at each confining pressure. These data are shown in Figure 5 with the sequence of the experiments indicated by arrows. One might expect that the permeability values of the first cycle would be slightly lower than the last values of the previous runs (around $35 \times 10^{-21} \text{ m}^2$ at a pressure difference of 10 MPa), continuing the downward trend observed in Figure 4. However, this was not the case; first cycle permeabilities were much higher ($107 \times 10^{-21} \text{ m}^2$ at a pressure difference of 10 MPa), nearer to the initial permeability values of the first run. Such behavior would indicate that there was some time-dependent factor that caused the permeability of the rock to increase during the 2-week hiatus, resulting in an apparent permeability recovery regardless of the applied confining pressure.

At a high pressure difference (95 MPa) the permeability of the two experimental series were quite similar. However, at a pressure difference of 10 MPa (comparing only the first three confining pressures) the range of values was greater in the first set of experiments than those conducted 2 weeks later (57 to $135 \times 10^{-21} \text{ m}^2$ versus 72 to $107 \times 10^{-21} \text{ m}^2$). This is because

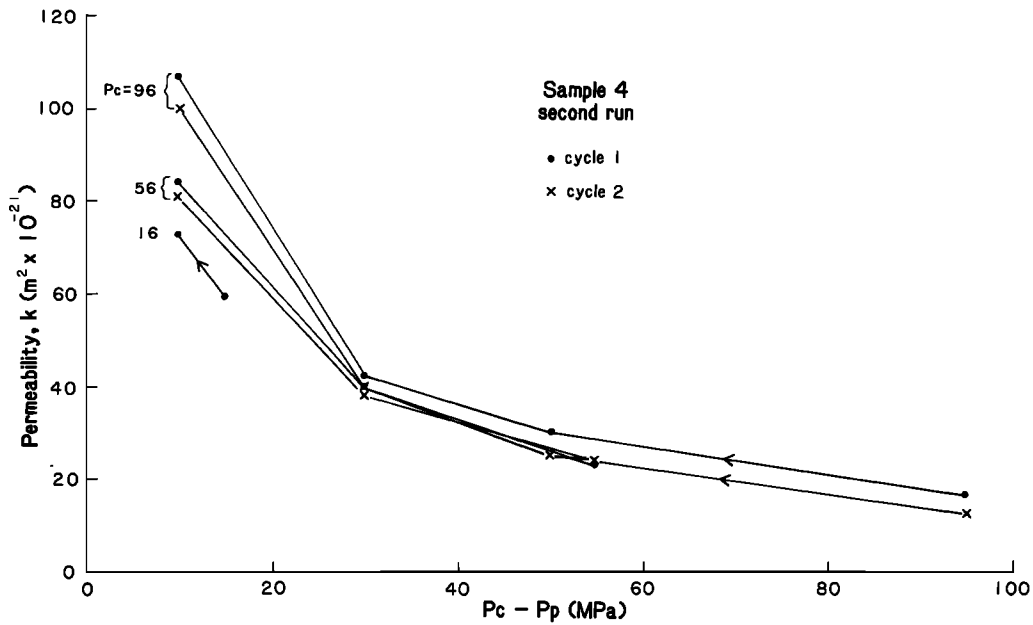


Fig. 5. Permeability as a function of pressure difference $P_c - P_p$ for sample 4, retested after an interval of 2 weeks at room pressure. Loading paths are shown with arrows. Confining pressures are listed at left. At the two higher confining pressures, pore pressure was loaded twice.

the permeability decreased for every loading cycle, and there were more cycles in the first test (three times loading and unloading) than in the second (twice, loading only).

DISCUSSION

In order to show that fluid flow through the rock follows the cubic root law (6), we need to find the appropriate effective stress factor α for Westerly granite. Two methods are discussed below.

1. When $k^{1/3}$ is plotted as a function of $\ln(P_e)$ with different values of α for each curve, we obtain a family of curves which are concave upward when α is low and concave down-

ward for high values of α . This procedure is illustrated in Figure 6 for the first loading cycle of sample 4, using extreme cases of α on the high and low sides. From this plot we can see that an α value of 1 gives the closest fit to a straight line of the three examples shown; α was calculated for sample 4 (56 and 96 MPa) by finding the value which minimized the standard deviation of the data points from a straight line in the $k^{1/3}$ versus $\ln(P_e)$ plot (see Table 2, graphic method); α was consistently close to 1, even though the permeabilities changed significantly. Values ranged between 0.95 and 1.14; however, the distribution is rather uneven, as a number of the values are equal to 1.01. There is no systematic trend in α for loading

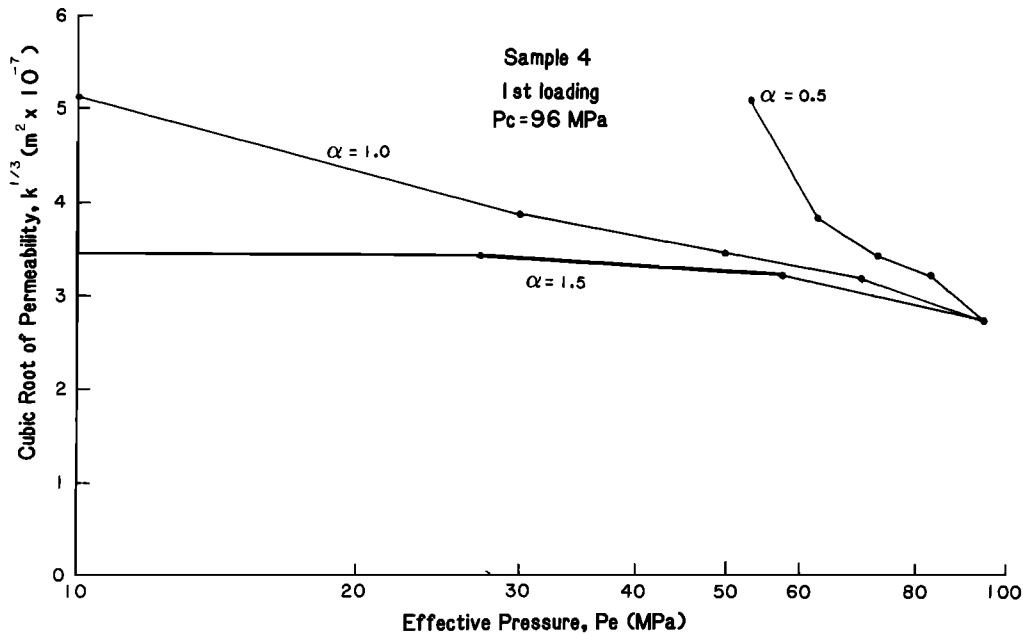


Fig. 6. Cubic root of permeability as a function of effective pressure for sample 4, first loading only, at a confining pressure of 96 MPa. By varying α , the line bends from concave upward (low α) to concave downward (high α); α is found when the deviations from a straight line are minimized, using a least squares fit.

TABLE 2. Values of α for Sample 4 Using Both the Graphical and Partial Differential Methods

Confining Pressure, MPa	Condition	α	
		Graphical	Differential
<i>Sample 4</i>			
96	cycle 1 load	1.04	1.03
	unload	1.00	0.98
96	cycle 2 load	1.01	0.96
	unload	0.95	1.00
96	cycle 3 load	1.04	1.04
	unload	1.01	1.01
56	cycle 1 load	1.01	1.00
	unload	1.01	1.04
56	cycle 2 load	1.03	1.02
	unload	1.07	1.13
56	cycle 3 load	1.14	1.23
	unload	1.09	1.16
<i>Sample 4 (Retested)</i>			
96	cycle 1 load	1.07	1.06
	cycle 2 load	1.04	1.03
56	cycle 1 load	1.01	1.00
	cycle 2 load	1.02	1.05

versus unloading conditions nor at the different confining pressures.

2. The α can also be found if we differentiate (6) with respect to pore pressure, as shown above

$$\frac{\delta(k^{1/3})}{\delta(P_p)} = -\frac{B\alpha}{P_c - \alpha P_p} \quad (7)$$

This derivative can be arranged to give the equation of a straight line:

$$P_p = B \left[\frac{\delta(P_p)}{\delta(k^{1/3})} \right] + \frac{P_c}{\alpha} \quad (8)$$

The derivative is obtained from the slope of a $k^{1/3}$ versus P_p plot at various values of intermediate pore pressures. From (8)

we see that a plot of pore pressure as a function of this partial gives a line with slope B and intercept P_c/α . This method was also used to find α for each cycle of sample 4, as shown in Table 2 under the differential method; α ranged between 0.96 and 1.23 and here again was independent of stress history. Based on the distribution of α given in Table 2, it would appear that the data toward the end of the first 56-MPa run are inconsistently high. The values for all other cycles of both runs fall at about 1.01 ± 0.06 . The differential method requires a sizeable data set (permeability measurements at many different pore pressures), in order to determine the partial derivative accurately. Otherwise, the slope of the function at a particular pore pressure can only be estimated from two distant data points. In addition, the number of partial derivatives that can be calculated is one less than the number of permeability measurements. In many cases only two points defined the line from which we obtain α . This limitation prevented us from calculating α at $P_c = 16$ MPa, where only one partial derivative could be determined.

From the methods of determining α discussed above, we conclude that most values fall in the range 1.01 ± 0.06 . Since the values were not dependent on either confining pressure or loading history, it would be most useful to simplify the effective stress equation to the form $P_e = P_c - P_p$, with $\alpha = 1$. Permeability and pressure data can now be plotted in the form of the cubic root equation (equation (6)) with the cubic root of permeability as a function of effective pressure (in this case, pressure difference). This is shown for samples 3 and 4 in Figures 7 and 8, respectively. Several features of these plots are immediately apparent. The data follow a linear relation between the two parameters for all pressure cycles. The slope B varied only slightly with each run. B , which from (4) is related to the quotient of the asperity height distribution h and aperture half width a_0 [Walsh, 1981], is not particularly sensitive to stress cycling effects because both h and a_0 are changing together and therefore their quotient remains fairly constant. A , on the other hand (related to permeability from (4)), is greatly effected by crack closure, permanent crack

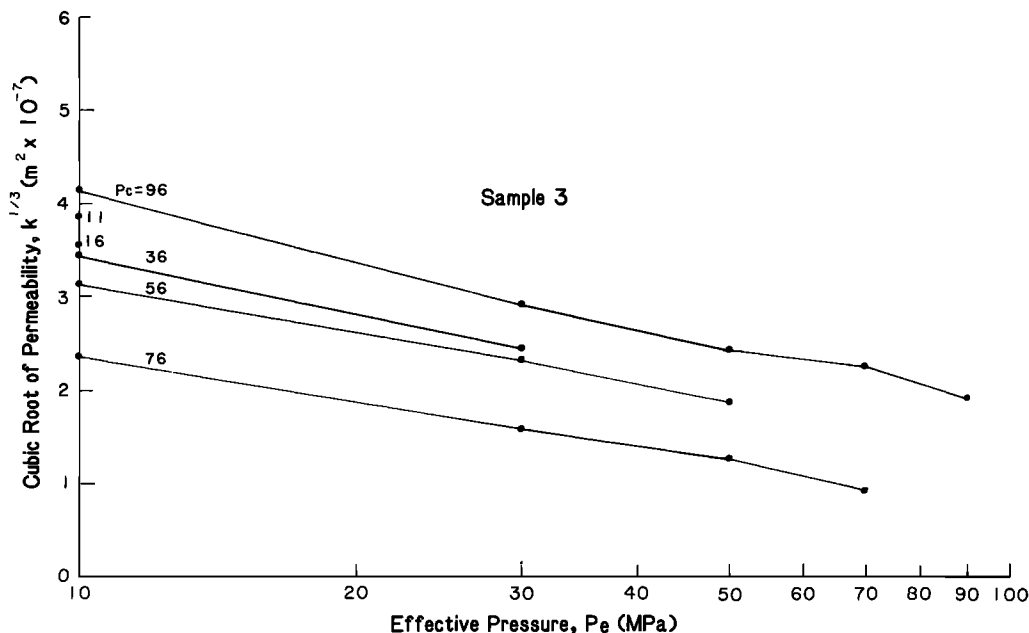


Fig. 7. Cubic root of permeability as a function of log effective pressure for sample 3; $\alpha = 1$ in this plot. Confining pressures are shown at left. These data follow the cubic root law, as $k^{1/3}$ is proportional to $\ln(P_e)$. The slope of the line gives the constant B of the cubic equation; the intercept gives A .

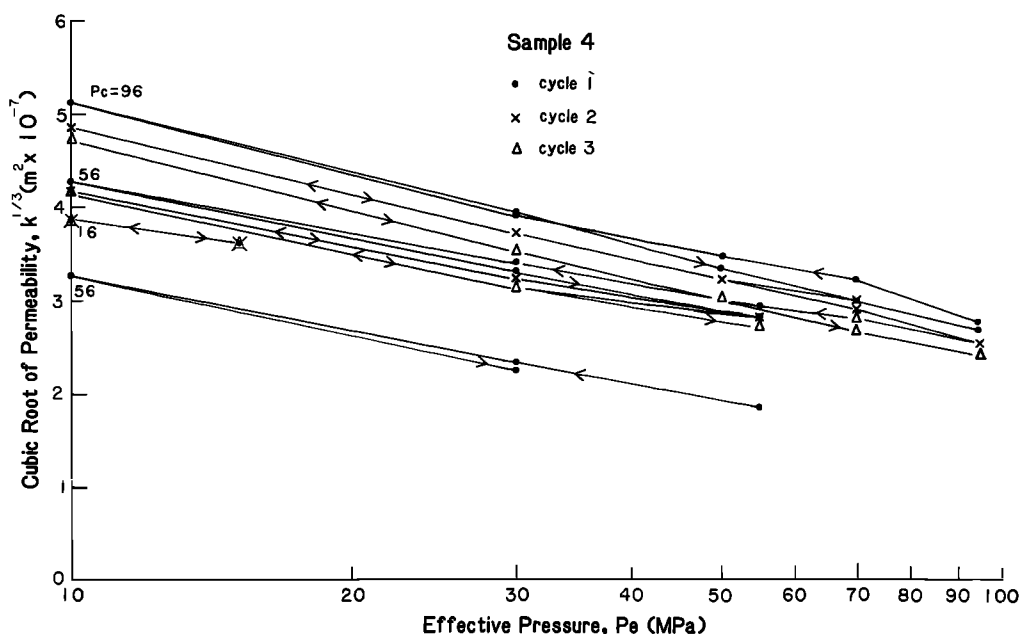


Fig. 8. Cubic root of permeability as a function of log effective pressure for sample 4. Confining pressures are shown at left, and loading paths are indicated by arrows. The first measurements begin with the uppermost line, right to left.

damage, or time-dependent relaxation effects. A decreased considerably during the experiments due to the stress cycling. This change was not permanent, as proven by the retest of sample 4. Therefore irreversible crack damage was probably not significant during the experiments, whereas stress relaxation effects became important with time. A decreased during the experiments because the stress relaxation was slow compared to the time frame of the tests.

These cycling effects lead us to conclude that the complete expression relating permeability to effective pressure must contain a stress history factor which we do not yet fully understand. These samples can be treated elastically according to (6) within each loading cycle. However, as a result of the cycling effects, permeability measurements at equivalent effective pressures for this granite do not necessarily yield the same results.

SUMMARY OF CONCLUSIONS

1. The constant α in the effective stress equation $P_e = P_c - \alpha P_p$ is about 1.01 ± 0.06 for Westerly granite under all conditions of pressure and loading history used here ($10 \text{ MPa} \leq P_c \leq 95 \text{ MPa}$). For simplicity, the effective stress equation can be reduced to the form $P_e = P_c - P_p$ in this case.

2. The permeability of Westerly granite is related to effective pressure according to the cubic root law, $k^{1/3} = A + B \ln(P_e)$ within each individual stress cycle.

3. Stress cycling had significant effects on the permeability of Westerly granite. Permeability decreased consistently with each loading, regardless of the confining pressure. However, a hiatus in the testing of sample 4 showed that stress relaxation counteracted these cycling effects, causing permeability to be higher than expected. It would appear that a more complete equation relating permeability to effective pressure must contain some stress history term that is not yet fully understood. As noted above, this stress cycling did not effect α .

REFERENCES

- Bernabé, Y., W. F. Brace and J. Walsh, Effective pressure law for permeability for two granites, *Eos Trans. AGU*, 65, 283, 1984.
- Bear, J., *Dynamics of Fluids in Porous Media*, p. 166, Elsevier, New York, 1972.
- Brar, N. S., and R. M. Stesky, Permeability of intact and jointed rock, *Eos Trans. AGU*, 61, 1112, 1980.
- Gangi, A. F., Variation of whole and fractured porous rock permeability with confining pressure, *Int. J. Rock Mech. Min. Sci. Geomech. Abstr.*, 15, 249-257, 1978.
- Jones, F. O., A laboratory study of the effects of confining pressure on fracture flow and storage capacity in carbonate rocks, *J. Pet. Technol.*, 27, 21-27, 1975.
- Lomize, G. M., *Flow in Fractured Rocks* (in Russian), 127 pp., Gose-nergoizdat, Moscow, 1951.
- Louis, C., A study of groundwater flow in jointed rock and its influence on the stability of rock masses, *Rock Mech. Res. Rep.* 10, 90 pp., Imp. Coll., London, 1969.
- Walsh, J. B., Effect of pore pressure and confining pressure on fracture permeability, *Int. J. Rock Mech. Min. Sci. Geomech. Abstr.*, 18, 429-435, 1981.
- Walsh, J. B., and M. A. Grosenbaugh, A new model for analyzing the effect of fractures on permeability, *J. Geophys. Res.*, 84, 3532-3536, 1979.
- Witherspoon, P. A., J. S. Y. Wang, K. Iwai, and J. E. Gale, Validity of Cubic law for fluid flow in a deformable rock fracture, *Water Resour. Res.*, 16, 1016-1024, 1980.
- Zoback, M. D., and J. D. Byerlee, Permeability and effective stress, *Am. Assoc. Pet. Geol. Bull.*, 59, 154-158, 1975.
- J. D. Byerlee and C. A. Morrow, U.S. Geological Survey, 345 Middlefield Road, MS/977, Menlo Park, CA 94025.
- Zhang B.-C., State Seismological Bureau, Beijing, Peoples' Republic of China.

(Received December 6, 1984;
revised May 13, 1985;
accepted November 1, 1985.)